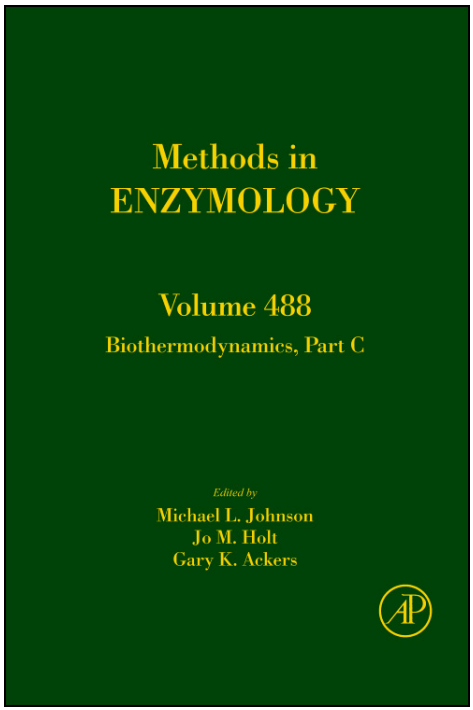

From: J. Ching Lee and Petr Herman, Structural and Functional Energetic Linkages in Allosteric Regulation of Muscle Pyruvate Kinase. In Michael L. Johnson, Jo M. Holt and Gary K. Ackers, editors: Methods in Enzymology, Vol. 488,
Burlington: Academic Press, 2011, pp. 185-217.
ISBN: 978-0-12-381268-1

CHAPTER EIGHT

Structural and Functional Energetic Linkages in Allosteric Regulation of Muscle Pyruvate Kinase

J. Ching Lee* *and* Petr Herman†

Contents

* Department of Biochemistry and Molecular Biology, The University of Texas Medical Branch at Galveston, Galveston, Texas, USA
† Institute of Physics, Charles University, Ke Karlovu, Prague, Czech Republic

Methods in Enzymology, Volume 488
ISSN 0076-6879, DOI: 10.1016/B978-0-12-381268-1.00008-2

Abstract

The understanding of the molecular mechanisms of allostery in rabbit muscle pyruvate kinase (RMPK) is still in its infancy. Although, there is a paucity of knowledge on the ground rules on how its functions are regulated, RMPK is an ideal system to address basic questions regarding the fundamental chemical principles governing the regulatory mechanisms about this enzyme which has a TIM $(\alpha/\beta)_8$ barrel structural motif [Copley, R. R., and Bork, P. (2000). Homology among $(\beta\alpha)8$ barrels: Implications for the evolution of metabolic pathways. *J. Mol. Biol.* **303,** 627–640; Farber, G. K., and Petsko, G. A. (1990). The evolution of $\alpha/ß$ barrel enzymes. *Trends Biochem.* **15,** 228–234; Gerlt, J. A., and Babbitt, P. C. (2001). Divergent evolution of enzymatic function: Mechanistically diverse superfamilies and functionally distinct superfamilies. *Annu. Rev. Biochem.* **70,** 209–246; Heggi, H., and Gerstein, M. (1999). The relationship between protein structure and function: A comprehensive survey with application to the yeast genome. *J. Mol. Biol.* **288,** 147–164; Wierenga, R. K. (2001). The TIM-barrel fold: A versatile framework for efficient enzymes. *FEB Lett.* **492,** 193–198]. RMPK is a homotetramer. Each subunit consists of 530 amino acids and multiple domains. The active site resides between the A and B domains. Besides the basic TIM-barrel motif, RMPK also exhibits looped-out regions in the α/β barrel of each monomer forming the B- and C-domains. The two isozymes of PK, namely, the kidney and muscle isozymes, exhibit very different allosteric behaviors under the same experimental condition. The only amino acid sequence differences between the mammalian kidney and muscle PK isozymes are located in the C-domain and are involved in intersubunit interactions. Thus, embedded in these two isozymes of PK are the rules involved in engineering the popular TIM $(\alpha/\beta)_8$ motif to modulate its allosteric properties. The PK system exhibits a lot of the properties that will allow mining of the ground rules governing the correlative linkages between sequence-fold-function. In this chapter, we review the approaches to acquire the fundamental functional and structural energetics that establish the linkages among this intricate network of linked multiequilibria. Results from these diverse approaches are integrated to establish a working model to represent the complex network of multiple linked reactions which ultimately leads to the observation of allosteric regulation of PK.

1. Introduction

Protein molecules are polyelectrolytes that are capable of binding ligands which would lead to biological activities or ligands which would regulate these activities, that is, proteins are involved in ligand bindings which can be expressed as linked multiequilibria (Steinhardt and Reynolds, 1969; Wyman and Gill, 1990). As a consequence of such a linkage, biological activities can be regulated exquisitely. In this chapter, we will address the applications of thermodynamics in the quest for the mechanism of the allosteric regulatory mechanism of allostery of an enzyme.

2. General Principles of Linked Multiequilibria Reactions

The following scheme is a generic expression of the thermodynamic cycle for a linkage of two equilibria of binding two ligands to protein P.

$$\begin{array}{ccc} & K_y & \\ X + P + Y & \rightleftharpoons & X + PY \\ K_x \uparrow\downarrow & & \downarrow\uparrow K_{x/y} \\ XP + Y & \rightleftharpoons & XPY \\ & K_{y/x} & \end{array}$$

Scheme 8.1 Thermodynamic cycle for linked reactions

where K_x and K_y are the binding constants of ligand X and Y to P in the absence of the second ligand, respectively. $K_{x/y}$ and $K_{y/x}$ are the binding constants of X and Y binding to P in the presence of saturating concentration of Y and X, respectively. If the presence of ligand X or Y affects the binding of Y or X, then those reactions are coupled. There are a few different ways to quantitatively express that relationship. They are:

2.1. Wyman linked function

The relation between equilibrium constants and effector concentration can be analyzed by the linked-function theory expressed by Tanford (1969)

$$\frac{\partial \ln K}{\partial \ln a_x} = \Delta v_x - \frac{n_x}{n_w}\Delta v_w = \Delta v_{x,\mathrm{pref}} \tag{8.1}$$

where K is the apparent binding constant of Y, a_x is the activity of effector ligand x, Δv_x and Δv_w are the changes in the amount of effector ligand and water, respectively, bound to P upon the change in states and n_x/n_w is the ratio of the number of moles of X to water present in the solution. Since n_x/n_w assumes a very small value, this term can be neglected. Then, measurement of binding constants of Y in the presence of varying concentrations of X can lead to an estimate of the nature of coupling between X and Y, be it positive or negative, that is, favoring of Y binding in the presence of X or *vice versa*.

2.2. Weber expression of the linked-function concept of Wyman in terms of binding energy

The term ΔG_{xy}, the free energy of interaction between ligands X and Y, is defined as (Weber, 1972)

$$\Delta G_{x/y} - \Delta G_x = \Delta G_{y/x} - \Delta G_y = \Delta G_{xy} \tag{8.2}$$

where ΔG_x and ΔG_y are the standard free energies of binding to unliganded P by X and Y, respectively, whereas $\Delta G_{x/y}$ and $\Delta G_{y/x}$ are the free energies of binding of X and Y to P which is fully liganded with the other ligand.

2.3. Reinhart derivation of the Weber expression as applied to steady-state kinetics

$$Q_{xy} = K_{x/y}/K_x = K_{y/x}/K_y, \quad \Delta G_{xy} = -RT\ln\left(Q_{xy}\right) \tag{8.3}$$

where the various terms for K have the same meaning as in Scheme 8.1. Application of this expression is valid only if it has been proven that the Michaelis constant, K_m, is equivalent to K_d, the dissociation constant of ligand binding. Readers are strongly recommended to review the elegant discussion of this application by Reinhart (2004).

ΔG_{xy} or Q_{xy} may assume either positive or negative values. This is a very valuable expression for a system that is just being investigated although these parameters do not provide information on the molecular mechanism of linkage. These coupling parameters expressed as such may include terms pertaining to conformational changes in protein P; change in protonation states of P as a result of binding of ligands, etc. For example, if P exists in an equilibrium between two conformation states, P and P′; each states can bind ligands albeit with different affinities, then in the presence of both X and Y, there are at least eight states that one needs to consider, namely, P, P′, PX, P′X, PY, P′Y, XPY and XP′Y. One is confronted with too many species to consider. Thus, it would be useful to simplify the system initially by

collecting terms related to these species into ΔG_{xy} or Q_{xy}. With additional studies using different approaches one might be able to identify and monitor the two protein states, P and P′. However, it will be most difficult to find distinctive structural properties for P, P′, PX, P′X, PY, P′Y, XPY and XP′Y so as to enable one to tract the presence of each of these states. The greatest challenge is to place the appropriate functional significance of those structural states. For example, a "minor" structural change which might be interpreted as insignificant but might represent a state that is functionally and energetically different. Thus, it is most fruitful to distinguish those intermediate states by classifying their energetics such as the elegant studies of Hb by Gary Ackers (Holt and Ackers, 1995).

3. Functional Energetic Linkages in Allosteric Regulation of Rabbit Muscle Pyruvate Kinase

Rabbit muscle pyruvate kinase (RMPK) is chosen as a model system to illustrate the various strategies that we have employed to study a specific phenomenon of linked multiequilibria, the allosteric regulation of this enzyme. The focus of this chapter is on solution energetics, thus most of the high resolution atomic structural information of RMPK is not presented. For readers who are more interested in the atomic structures of RMPK or other isozymes of PK, they should consult the pioneering work by Muirhead, Reed, Rayment, Mattevi, and their coworkers (Larsen *et al.*, 1994, 1997, 1998; Mattevi *et al.*, 1995, 1996; Stuart *et al.*, 1979). More recently, the work of Fenton and Mesecar should also be consulted (Dombrauckas *et al.*, 2005; Williams *et al.*, 2006).

RMPK is an important allosteric enzyme of the glycolytic pathway catalyzing a transfer of the phosphate from phosphoenolpyruvate (PEP) to ADP (Ainsworth and MacFarlane, 1973; Consler *et al.*, 1989, 1992; Hall and Cottam, 1978; Oberfelder *et al.*, 1984a,b)

$$\text{PEP} + \text{ADP} \rightarrow \text{pyruvate} + \text{ATP}$$

RMPK has a TIM $(\alpha/\beta)_8$ barrel structural motif (Copley and Bork, 2000; Farber and Petsko, 1990; Gerlt and Babbitt, 2001; Heggi and Gerstein, 1999; Wierenga, 2001). The enzymatic reaction requires two metal ions, namely, K^+ and Mg^{2+}; it is inhibited by Phe or other amino acids and activated by phosphofructose 1,6-bisphosphate (FBP). Production of ATP is essential in the cell energetics, and therefore, it is not surprising that RMPK activity is subjected to an intriguing pattern of regulation. RMPK consists of four identical subunits (Larsen *et al.*, 1994; Stuart *et al.*, 1979) each of which is composed of three domains, A, B, and C. The binding sites of various ligands are distributed at distant regions of the molecule, as shown in Fig. 8.1. Thus, the

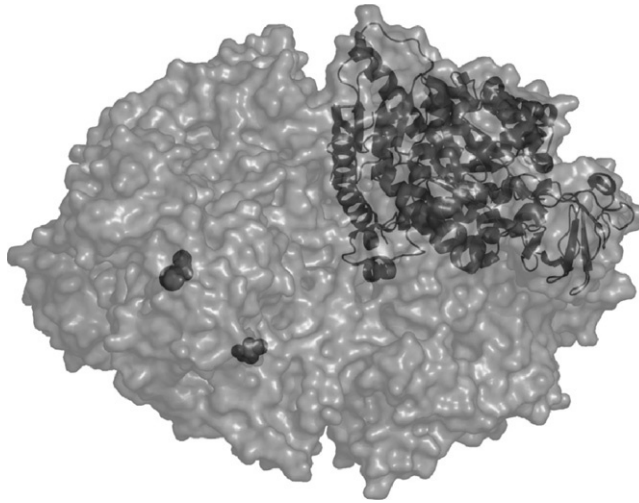

Figure 8.1 Tetrameric structure of RMPK. One of the subunits is presented as cartoon over the surface presentation. The spheres are representations of the distance between the active site and the binding site of inhibitor. The structure is generated using the coordinates of Wooll *et al.* (2001).

mechanism of communication must involve long-range communications between these distant sites. An elucidation of the regulatory mechanism must consider the linked multiequilibria interactions linking subunit–subunit communications, interfacial interactions among these domains and effects of binding of these various ligands on these macromolecular interactions. We will illustrate the various strategies that have been successfully applied to RMPK.

The minimum ligands that are important for RMPK activity include:

- Substrates: PEP and ADP
- Metal cofactors: K^+ and Mg^{2+}.
- Inhibitor: Phe and other amino acids
- Activator: FBP
- Solution environmental effects: pH and temperature.

Thus, it is immediately obvious that the basic regulatory mechanism for RMPK is complex and the investigator needs to elucidate the linkages among bindings of at least seven ligands (H^+ is also a ligand) and their effects on interfacial interaction or the reciprocal effects.

4. Functional Linkage Through Steady-State Kinetics

A useful approach to initiate a general mapping of the allosteric behavior of an enzyme system is through steady-state kinetics, which in the present case with RMPK the measurements are conducted with the

coupled enzyme assay. In such a case, it is essential to ascertain that the observed kinetic behavior is a true reflection of RMPK and not influenced by the coupling enzyme, lactate dehydrogenase. Control experiments were conducted in all of the experimental conditions by monitoring the activity versus substrate concentration relation as a function of lactate dehydrogenase concentration ranging from 5 to 20 μg/mL. In all of the experimental conditions, namely, pH ranging from 6.0 to 9.0 in the absence and presence of Phe, there are no quantitative differences in the activity substrate concentration relations regardless of the concentration of lactate dehydrogenase. These results show that the coupling enzyme is not a limiting factor, and the kinetic results do reflect the intrinsic behavior of RMPK.

4.1. H^+ effect

The steady-state kinetics of RMPK was studied as a function of pH ranging from 6.0 to 9.0 in the presence of Phe concentrations ranging from 0 to 20 m*M*. In the absence of Phe, the value of $K_{m,app}$, the K_m value at a specific experimental condition, shows only a slight dependence on pH. However, the presence of Phe significantly affects the value of $K_{m,app}$, which increases with increasing pH. In earlier studies, it has been shown that $1/K_{m,app}$ can be approximated as the apparent dissociation constants of PEP, $K_{d,app}$ (Oberfelder *et al.*, 1984a,b). Thus, the dependence of $K_{m,app}$ on pH can be analyzed by the Wyman linked function (1964). The relation between equilibrium constants and effector concentration can be analyzed by the linked-function theory expressed by Tanford (1969) as shown in Eq. (8.1). In the absence of Phe, $\Delta v_{H^+} = 0.16$, that is, RMPK activity is linked to a net absorption of H^+. However, this analysis does not provide information on the source and nature of this change.

4.2. Coupling reaction between H^+ and Phe

This set of data consists of RMPK activity as a function of H^+ in the presence of varying concentrations of Phe. The data can be analysis by the Wyman linked function. In all cases, the slope yields positive values for Δv_{H^+} and increases with increasing Phe concentration. The values of Δv_{H^+} range from 0.16 ± 0.03 to 0.83 ± 0.08 within the Phe concentration range of 0–20 m*M*. These results imply that in converting RMPK to the active form by PEP, a net absorption of proton is observed, although the magnitude of change depends on the amount of Phe present. An analogous analysis was applied to the data with Phe as the variable ligand. Under all pH values tested, Δv_{Phe} assumes a negative value which becomes more negative with increasing pH until it assumes an apparently maximum value of 1.0. These results imply that conversion of RMPK to the active form in

the assay mixture requires a release of Phe, the amount of which is pH dependent. Thus, the effects of H^+ and Phe are antagonistic to each other.

4.3. Coupling reaction between PEP and Phe

The relation between the apparent binding constants of PEP and Phe concentration was further analyzed by the linked function in accordance with Eq. (8.1) and a slope of -0.9 was obtained. This value suggests that the binding of an additional mole of PEP results in a net release of about 1 mol of Phe.

4.4. Coupling reactions between metal ions and other metabolites

The enzymic activity of RMPK requires the presence of both K^+ and Mg^{2+}. However, other divalent cations have been used to replace Mg^{2+}. Depending on the source of the PK under investigation, the allosteric properties may be altered when Mg^{2+} is replaced by Mn^{2+} (Larsen *et al.*, 1994, 1997; Suelter *et al.*, 1966). Mesecar and Nowak (1997a,b) tested the linkage of divalent metal ions on yeast PK activity. These investigators applied the Reinhart expression of linked function to analyze the results of their studies. Their results show that Mn^{2+} is energetically coupled to the binding of PEP and FBP. The coupling energy to PEP and FBP are -2.75 and -1.55 kcal/mol, respectively. The negative coupling energy indicates that the presence of Mn^{2+} would favor the binding of PEP and FBP. However, there is no observable coupling energy between the bindings of FBP and PEP. Thus, the coupling mechanism between observed positive cooperativity in PEP and FBP bindings is the consequence of an indirect coupling through Mn^{2+}, a novel observation, since the locations of the binding sites of these two molecules are many Å apart.

Fenton and Alontaga (2009) conducted an extensive study on the effects of mono- and divalent cations on the binding of PEP, FBP, and inhibitor alanine to human liver PK. By applying the Reinhart expression to their steady-state kinetic data, the authors convincing demonstrated the impact of cations and anions on the allosteric behavior of liver PK. The magnitude of coupling is dependent on the identity and concentration of these ions. Thus, modulation of the complex allosteric behavior in PK is the net consequence of an intriguing and complex network of coupling among multiequilibria linked reactions. Fenton and Hutchison (2009) further studied the coupling between H^+ and other metabolites such as FBP, ATP, and Ala in human liver PK.

4.5. Dissecting the thermodynamic contribution of Phe binding

Fenton and coworkers applied the Reinhart expression to their steady-state kinetic data in the presence of various structural analogues of Phe to pin point the driving forces of various structural moieties of Phe in eliciting the inhibitory behavior (Williams *et al.*, 2006). Through this extensive and meticulous study they concluded that the L-2-aminopropanaldehyde substructure of the amino acid ligand is primarily responsible for binding to RMPK and hydrophobic interaction is the driving force of this interaction. They further determined the structure of the RMPK–Ala complex, thus is able to identify the inhibitor binding site.

5. Structural Perturbations by Ligands

The powerful linked-function analysis illustrates the usefulness of the approach in providing a quantitative indication of the nature of coupling between multiple linked reactions. In general, it is an accepted concept that protein structural changes are an integral part of allosteric mechanisms (Koshland *et al.*, 1966; Monod *et al.*, 1965). The physical identities of these states are not defined in these hypotheses, although it has been generally accepted that they are manifested as changes in secondary–tertiary structures of the enzyme. For the RMPK system, there is substantial spectroscopic evidence in the literature demonstrating that some chromophores in RMPK are perturbed by effectors and substrates (Kayne, 1973; Kayne and Price, 1972; Kwan and Davis, 1980, 1981; Suelter *et al.*, 1966). However, there have been no attempts to quantitatively relate structural changes to the enzyme kinetic observations. Since we know that kinetic and equilibrium binding data alone *do not* provide enough information to establish a molecular model for the allosteric behavior of RMPK, an extensive study was made to quantitatively correlate the change in the global RMPK structure with enzyme kinetic and ligand binding observations. The goal is to elucidate the mechanism through which allosteric regulation is elicited.

A prerequisite to developing a molecular model of allosteric regulation requires additional information to identify the structural components that are included in the general term of $\Delta v_{x,\,pref}$, ΔG_{xy}, or Q_{xy}. These structural changes may include subunit association–dissociation and domain movements. In the studies of RMPK, the specific goal is to address changes in hydrodynamic properties instead of detail atomic level information such as those revealed by spectroscopic techniques because it is difficult to dissect the spectroscopic data to distinguish changes in quaternary structures from

local environmental changes around the probe. The hydrodynamic properties enable the investigator to monitor changes in solution as a function of variables such as ligand binding.

5.1. Subunit interaction by sedimentation equilibrium

Both the kinetic and ligand binding data indicate that RMPK exhibits allosteric properties in the presence of Phe; however, the physical identities of the different states of the enzyme implied by these data remained to be determined. These states might be oligomeric forms of RMPK differing from one another in their degrees of polymerization. This possibility was tested by monitoring the molecular weight of RMPK in the presence and absence of Phe by sedimentation equilibrium (Oberfelder *et al.*, 1984a). Within the concentration range of 50–750 μg/mL, the value for the weight-average molecular weight is the same as that of the number-average molecular weight, suggesting that the protein in solution is homogeneous. There is little discernible difference between the data sets obtained in the presence or absence of Phe. The average molecular weight of RMPK is shown to be 220,000 ± 5000, which is not dependent on protein concentration. These results imply that native RMPK does not undergo association–dissociation under the conditions tested. This conclusion is further substantiated by sedimentation velocity data at protein concentrations as low as 15 μg/mL. The sedimentation coefficient did not show any evidence of a dependence on protein concentration. Thus, the states of RMPK do not involve association–dissociation of this tetrameric enzyme.

5.2. Differential sedimentation velocity

Since the tetrameric RMPK does not undergo association–dissociation, the different states in the allosteric model are likely manifestations of secondary–tertiary structural changes in the enzyme. Evidence for such a change was sought through fluorescence, chemical modification, and difference sedimentation velocity experiments (Oberfelder *et al.*, 1984a). These methods were chosen to monitor different levels of structural changes which might be ligand dependent; for example, the sedimentation experiments would yield information on the global structural changes while the other experiments might indicate more localized structural changes.

The change in hydrodynamic properties of RMPK induced by ligands was monitored by difference sedimentation velocity with a Beckman analytical ultracentrifuge according to the procedure of Gerhart and Schachman (1968). For each experiment, two double-sector cells were placed in a rotor. One cell contained RMPK in the presence of the ligand being tested, while the other cell contained RMPK in the presence of tetramethylammonium chloride, the concentration of which was adjusted

to an ionic strength equivalent to that of the test ligand. The difference in sedimentation coefficients, ΔS, can be computed with the following equation (Howlett and Schachman, 1977):

$$\frac{1}{\omega^2}\frac{\partial(\Delta r/\bar{r})}{\partial t} = \Delta S \tag{8.4}$$

where ω is the angular velocity, $\Delta r = r_2 - r_1$, $\bar{r} = (r_1 + r_2)/2$, and t is time. r_2 and r_1 are the radial positions of the peaks of the sample and reference solution, respectively. The reported sedimentation coefficients were corrected to the standard conditions of 20 °C in water. The densities and viscosities of the buffer and ligand-containing solutions were measured with a precision density meter and viscometer, respectively.

Difference sedimentation experiments were performed as a function of the Phe concentration in 50 m*M* Tris at pH 7.5. These experiments were conducted to monitor the effect of Phe on RMPK in the absence of any activators. Results of these experiments show a decrease in $s_{20,w}$ and the value of $\Delta s_{20,w}$ reaches a maximum of -0.24 S at infinite concentrations of Phe. The effect of activating cations of Mg^{2+} and K^+ on the Phe-induced structural change was also monitored. The sedimentation rates of all of the Phe-containing samples were slower than those of the reference solutions. The change is dependent on Phe concentration and approaches a maximum value of -0.13 S at infinite concentrations of Phe. Thus, there are coupling between activating cations and Phe, as reflected by the difference in the change in hydrodynamic properties of RMPK, namely, -0.24 and -0.13 S without and with Mg^{2+} and K^+, respectively. The effects of a variety of other ligands on the hydrodynamic properties of PK were also tested. PEP apparently produces an increase in the sedimentation rate while the other substrate, ADP, did not appear to induce any significant changes. $MgSO_4$ and KC1 individually produce small increases in the sedimentation rate, but together they induce a more substantial increase. Hence, there seems to be coupling between Mg^{2+} and K^+ bindings. Although Ala itself does not induce any significant change in the hydrodynamic properties of RMPK, it does reverse the structural change in RMPK induced by Phe. When RMPK alone was used as a reference, 100 m*M* TMA^+Cl^- produced an increase in the sedimentation rate after correction for changes in viscosity and density. The result with TMA^+Cl^- suggests that there may be a nonspecific ionic strength effect at relatively high ionic strengths which results in an increase in the sedimentation rate.

Having established that Phe induces a global structural change in RMPK, it is *important to compare the structural and equilibrium binding data to establish a molecular model which best fits all of the data*. If the Phe-induced state change is completed prior to saturation of the binding sites by the ligand,

then a model that involves a concerted structural change is the likely explanation for the observed phenomenon. On the other hand, if the state change coincides with the binding isotherm, a sequential model is suggested. In order to facilitate comparison of the data, both the state change and binding data were expressed as fractional changes. This comparison shows that the completion of state change *precedes* the saturation of Phe binding. At 0.5 m*M* Phe, the state change is greater than 80% complete while the protein is only 25% saturated with the ligand. Since there are four binding sites of Phe per RMPK tetramer, this result indicates that the binding of 1 mol of Phe results in a shift of the state equilibrium to the point where the transition is greater than three-quarters complete. On the basis of this evidence, the two-state model seems to be the most likely one to describe the observed phenomena (Oberfelder *et al.*, 1984a).

Phe binding is clearly linked to the state change in RMPK, so it is of interest to investigate the relation quantitatively. Let us assume that the fractional change in $\Delta S_{20,w}$ represents the relative distribution between the two states, R and T, so that

$$\frac{\Delta S_{20,w}}{\Delta S_{20,w,max} - \Delta S_{20,w}} = \frac{T}{R} = K_{R \leftrightarrow T} \tag{8.5}$$

where $\Delta S_{20,w}$ and $\Delta S_{20,w,max}$ are the observed change in the sedimentation coefficient at a particular Phe concentration and the maximum change of the sedimentation coefficient at infinite Phe concentration, respectively. T and R are the concentrations of the two proposed states of RMPK, and $K_{R \leftrightarrow T}$ is the equilibrium constant characterizing the transition between states. The relation between equilibrium constants and Phe concentration can be analyzed by the linked-function theory expressed by Tanford (1969), Eq. (8.1), where a_x is the activity of Phe, Δv is the change in the amount of Phe bound per tetrameric RMPK upon a change in states, and n_{Phe}/n_w is the ratio of the number of moles of Phe to water present in the solution. Since n_{Phe}/n_w assumes a very small value, this term can be neglected from Eq. (8.1). The result of such an analysis shows a slope of $+0.7$, thus suggesting that the occurrence of a state transition from R to T involves a net uptake of about 1 mol of Phe.

The present study provides evidence that the interactions between RMPK and ligands are closely linked to the state change.

5.3. Analytical gel filtration chromatography

The differential sedimentation velocity technique is capable of monitoring minute changes in hydrodynamic properties of RMPK, however, the concentration of protein required is in the mg/mL regime which is an

order of magnitude above the estimated *in vivo* concentration of the protein. Thus, analytical gel filtration chromatography is employed (Heyduk *et al.*, 1992). This technique enables one to determine the hydrodynamic properties at μg/mL or lower concentrations. Briefly, buffer and protein solution were held in containers A and B, respectively, which are connected through a two-way tap with a thermostated chromatography column equipped with an adaptor. The eluent can be monitored by fluorescence with the aid of a flow cell with a capacity of 300 μL. Fluorescence detection allows the use of much lower protein concentrations and minimization of interference by Phe. The solution from the flow cell passes to a pump and finally to a weighing bottle for measuring flow rate. All connecting tubings were kept as short as possible. After equilibration with buffer, at least 10 ml of protein solution was then applied to the column via the two-way valve, ensuring that the conditions required for a large zone experiment were fulfilled. A large zone has to be used in order to obtain thermodynamically valid results for interacting systems (Ackers, 1970). Application of protein solution to the column has to be precisely correlated with the start of monitoring of the effluent by fluorescence. Two thousand data points were collected for each elution profile. The raw data in the form of fluorescence intensity as a function of time of elution were converted to fluorescence intensity as a function of volume of eluent, using the measured flow rate. Since a precise measurement of the flow rate is critical in these experiments, it has to be individually measured for each experiment by weighing the effluent collected from the start of recording to the appearance of a boundary. Elution volumes were determined as the centroid of the leading boundary. The centroid is defined as the elution volume at which areas for each boundary below and above solute profile are equal (Ackers, 1970). Base lines were calculated by linear regression performed on the linear portions of the elution profile. When the elution volumes of protein in the absence and presence of ligand were to be compared, the experiment with the protein in buffer was conducted first on a column equilibrated with buffer. The column was then reequilibrated with buffer in the presence of ligand.

The performance of a Pharmacia C10/40 column with a bed volume of 25 ml was monitored. For consecutive runs performed on the same sample on the same day, elution volume was reproducible to ± 7 μL (standard deviation of mean value), whereas the long term stability within a period of several weeks was ± 50 μL. The precision on determining the difference in elution volume in the presence and absence of ligand was ± 15 μL which means that for a protein of the size of 45 kDa (about 28 Å), it should be possible to detect changes of > 0.1 Å, that is, $> 0.4\%$ of the Stokes radius.

For RMPK Sephacryl 300 HR columns were calibrated with ribonuclease A, chymotrypsinogen A, ovalbumin, aldolase, and ferritin. *N*-Acetyltryptophan amide and blue dextran were used to determine the total

volume (V_t) and the void volume (V_o) of the column, respectively. The partition coefficient, K_{av}, is calculated as

$$K_{av} = (V_e - V_o)/(V_t - V_o) \tag{8.6}$$

where V_e is the elution volume of the protein. Plotting Stokes radii of standard proteins as a function of $(-\log K_{av})^{1/2}$ (Siegel and Monty, 1966) yielded a straight line, which is used to calculate the Stokes radii. The differences in elution volume (ΔV) between RMPK in the absence and presence of Phe were monitored as a function of Phe concentration. The elution volume of the RMPK–phenylalanine complex is less than that of RMPK alone, as indicated by a positive change in ΔV. This result shows that the RMPK–Phe complex exhibits a larger Stokes radius, that is, more asymmetric or expanded, which is an observation that is in total agreement with that from a study using neutron scattering (Consler *et al.*, 1988) and differential sedimentation velocity (Oberfelder *et al.*, 1984a).

It is possible to predict the distribution between R and T states in a set of concentrations of Phe by using these constants in the following equation (Oberfelder *et al.*, 1984b).

$$\bar{T} = L\left(1 + [\mathrm{I}]/K_{\mathrm{I}}^{\mathrm{T}}\right)^4 / \left(1 + [\mathrm{I}]/K_{\mathrm{I}}^{\mathrm{R}}\right)^4 + L\left(1 + [\mathrm{I}]/K_{\mathrm{I}}^{\mathrm{T}}\right)^4 \tag{8.7}$$

where L is the intrinsic allosteric equilibrium constant, $\bar{T}$ is the fraction of molecules in the T state, [I] is Phe concentration and superscripts R and T in the equilibrium constants (K) specify the conformational state of the protein. Using the equilibrium constants derived from kinetic data (Consler *et al.*, 1989) in combination with the equation

$$\Delta V = \Delta V_{\max}(\bar{T} - \bar{T}_0)/(1 - \bar{T}_0) \tag{8.8}$$

where $\bar{T}_0$ is the fraction of T in the absence of Phe, a curve was generated to express difference in elution volume ΔV as a function of Phe concentration. Values for the different constants used are $L = 0.06$, $K_{\mathrm{I}}^{\mathrm{R}} = 13$ mM, and $K_{\mathrm{I}}^{\mathrm{T}} = 0.78$ mM. The predicted data are not in good agreement with that of the experimental data, and a systematic deviation was observed. A search was undertaken to determine the values for these equilibrium constants that would best fit the experimental data. The results that lead to a perfect fit include the values $L = 0.094$, $K_{\mathrm{I}}^{\mathrm{R}} = 13$ mM, and $K_{\mathrm{I}}^{\mathrm{T}} = 0.4$ mM. These values are within the standard deviations of these constants determined by steady-state kinetics (Consler *et al.*, 1989). The coincidence of the simulated plot with the experimental data provides a strong credence to the validity of the two-state model adopted for the RMPK system, because the simulated plot is based entirely on parameters obtained from the analysis of kinetic data

and the hydrodynamic experimental data are directly related to a global conformation change of the enzyme. In a separate experiment, the observed value of ΔV_{max} corresponds to a change of 1.2 Å, in Stokes radius. This correlates very well with a change of 1–2 Å in the radius of gyration observed by small angle neutron scattering (SANS) under similar experimental conditions (Consler *et al.*, 1988). In accordance with Eq. (8.3) and the equilibrium constants reported by Consler *et al.* (1989), it is possible to predict the effect of PEP upon its addition to a mixture of RMPK and Phe. PEP should shift the equilibrium toward the R state and, therefore, one should observe a shift of the elution volume of RMPK toward larger values, that is, in the presence of PEP, ΔV should be smaller than that in the presence of Phe alone and, in low concentrations of Phe, can actually become negative. Experimental results with 0.5 and 5 m*M* Phe in the presence of 0.1 m*M* PEP confirm this prediction. These results show that RMPK undergoes a concerted global structural change and the binding of Phe follows a positive cooperativity mode.

5.4. Small angle neutron scattering or small angle X-ray scattering

To characterize this change in global structure of RMPK, we studied the effects of ligands on the structure of RMPK by SANS (Consler *et al.*, 1988). The radius of gyration, R_G, decreases by about 1 Å in the presence of substrate PEP but increases by the same magnitude in the presence of inhibitor Phe.

5.4.1. The SANS data can be subjected to two separate analyses

The first method relies upon the data obtained at the lower scattering angles. Data in this region conform to the Guinier relationship:

$$\ln I(k) = -k^2 R_G^2/3 + \ln I(0) \tag{8.9}$$

where $I(k)$ and $I(0)$ are the scattering intensities at angles 2θ and 0, respectively, $k = (4\pi \sin \theta)/\lambda$, and R_G is the radius of gyration. From a Guinier plot of ln $I(k)$ versus k^2, one is able to determine R_G and $I(0)$. Data points from low angle scattering up to $k = 0.07$ Å^{-1} will be subjected to weighted linear least-squares fitting to yield values for these two parameters. The radius of gyration, R_G, decreases by about 1 Å in the presence of substrate PEP but increases by the same magnitude in the presence of inhibitor Phe.

The second method of analysis takes into account all of the SANS data up to the point where the intensity approaches 0, for example, up to $k = 0.13$ Å^{-1}. The analysis yields the length distribution function, which is defined by Eq. (8.10).

$$P(r) = (2r/\pi) \int_0^\infty kI(k)\sin(kr)\,\mathrm{d}x \tag{8.10}$$

where $P(r)$ is the frequency distribution of all the point-to-point pair distances, r, between scattering centers of the particle. This function can be approximated by the indirect transform method of Moore (1980) and yields information that describes the size, shape, and frequency distribution of all the point-to-point pair distances between scattering centers of the particle. It also yields values for R_G. Since this analysis utilizes more of the scattering data than the Guinier analysis, it contains more information. When the scattering data were analyzed as a function of $P(r)$ versus r, the results indicate that the increase in R_G is associated with a pronounced increase in the probability for interatomic distance between 80 and 110 Å.

5.4.2. Comparison of solution and crystal structures

Using the α-carbon coordinates determined by X-ray crystallography, the solution scattering behavior of the observed conformation of RMPK was predicted. The scattering curve and $P(r)$ distribution were calculated from the known α-carbon coordinates as follows. The coordinates for the symmetric tetramer were constructed by applying the appropriate symmetry operations to the crystallographic monomer coordinates. For an object assumed to consist of discrete density points, the Debye (1915) relation can be used to calculate the scattering curve directly. All coordinate pairs were used to directly calculate $P(r)$ for RMPK, in this calculation, the scattering length density was assumed to be uniformly constant throughout the molecule.

The fact that the observed scattering data contain information pertaining to interatomic distances enables one to generate length distributions from both SANS and X-ray crystallographic data. The changes in length distributions, reflecting conformational changes induced by ligands, can then be compared between the two sets of experimental observations. It must be stressed that separate comparisons were conducted for the structural parameters derived from solution and the crystal structure. Our approach thus involves generating the difference distribution, $\Delta P(r)$, which is ideal for the comparison of data sets obtained under different conditions. This function ($\Delta P(r)$) enables one to determine the (length distribution) changes that occur in solution. Once those changes are determined, they are used as a guideline for the modeling that involves manipulation of the α-carbon coordinates. The computation is deemed satisfactory when it yields a $\Delta P(r)$ function that compares favorably with that determined from solution data. A series of calculations and simulations were carried out. The common element in the analysis is the relationship of I versus k. This is obtained directly from SANS, and indirectly from X-ray crystallographic coordinates through the Debye (1915) relationship. Once the three-dimensional

coordinate data are converted to the form of an I versus k distribution, the path of data analysis converges, since both solution and crystal data are treated identically. This simulation step employed computer graphics, which enabled us to conduct interactive rotation and translation, symmetry operations, and inter-α-carbon distance calculations. Having decided on a simulated conformational change, the information was then reintroduced into the path of data analysis in the form of altered α-carbon coordinates. All manipulations on the α-carbon coordinates were performed on isolated monomers. Subsequently, these newly modeled structures were used to reconstruct the tetramer by the same symmetry operations that yielded the original tetramer. The point at which the comparison between experimental and simulated data takes place is at the level of $P(r)$ distribution.

The difference between solution conformations, $\Delta P(r)_{\text{solution}}$, and crystal conformations, $\Delta P(r)_{\text{crystal}}$, was compared; when $\Delta P(r)_{\text{solution}} = \Delta P(r)_{\text{crystal}}$, the conformational change was considered adequately modeled. This approach is especially useful for the comparison of data sets obtained under different solution conditions. Hence, $P(r)$ distributions were employed to illustrate changes in molecular dimensions that are the result of these solution variations.

With the aid of computer modeling, these changes in interatomic distance is consistent with the rotation of the B domain relative to the A domain, leading to the closure or opening of the cleft between these domains as a consequence of binding to PEP and Phe, respectively. These results show that one of the dynamic motions in RMPK includes change in domain–domain interaction between A and B domains.

6. Functional Linkage Scheme of Allostery for RMPK

As a result of a series of extensive steady-state kinetic, equilibrium, and solution structural studies, a concerted, allosteric model was developed for quantitative interpretation of the kinetic and equilibrium binding data of RMPK (Consler *et al.*, 1888, 1992; Heyduk *et al.*, 1992; Oberfelder *et al.*, 1984b; Yu *et al.*, 2003). The simplest model accounting for all the experimental data involves two conformational states, inactive E^T and active E^R, shown in Fig. 8.2. E, S, P, and I are enzyme, substrate (PEP or ADP), product (pyruvate), and inhibitor (Phe), respectively.

The upper and lower faces of the cube contain all of those species assuming E^R and E^T state, respectively. The species are interconnected with equilibrium constant, $L = [E^T]/[E^R]$; K^R and K^T are the ligand binding equilibrium constants associated to the E^R and E^T state, respectively, while K_I and K_S are the equilibrium constants associated with the

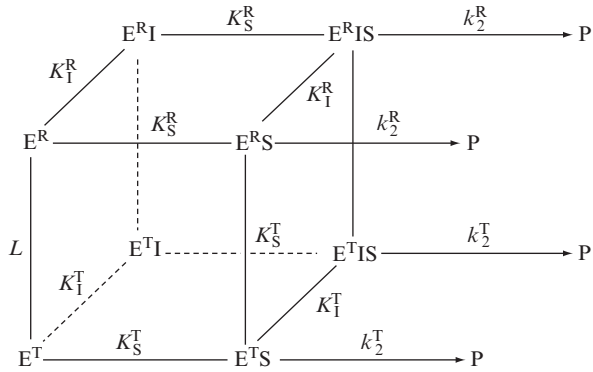

Figure 8.2 The proposed two-state model for the allosteric behavior of RMPK (Oberfelder *et al.*, 1984b). $L = [T] / [R]$; K^T and K^R are equilibrium constants for substrates, S, and inhibitor, I, binding to the T and R state, respectively. The model assumes that the affinities of RMPK for both S and I are dependent only on the conformational state of the enzyme, that is, the constant for the binding of S to E^T is the same as that of S to $E^T \cdot I$. Similarly, the affinity of S for E^R and $E^R \cdot I$ is assumed to be the same.

binding of inhibitor Phe and substrate, respectively. The conceptual significance of this model is that the two states are in a preexisting equilibrium, L. This crucial aspect of the model was independently substantiated by the literature (Harris and Winzor, 1998). The distribution of ligands bound to these two states is defined by their respective equilibrium constants to these states. The ligands shift the state changes in PK by mass action. This model differs from models which assume a mechanism consisting of a ligand induced state change not in a preexisting equilibrium.

The simple model shown in Fig. 8.2 is NOT adequate to account for the experimentally defined energy landscape of the linked equilibria that govern the enzymatic reactions. Added novel features are derived from global analysis of calorimetric and fluorescence data (see Section 7.5 for further discussion).

7. Functional Linkage Through Ligand Binding Measurements

As useful as the steady-state kinetic analysis, it is imperative to verify the quantitative parameters determined by measuring the energetic of ligand binding. Both direct (equilibrium dialysis or equivalent) and indirect (fluorescence and isothermal titration calorimetry) methods were employed in our studies.

7.1. Equilibrium binding

The binding of ligand to RMPK can be measured by the method of Hirose and Kano (1971). The advantage of this approach or its equivalent is the ability to keep the concentration of P constant. This is particularly important for proteins that may undergo association–dissociation (Na and Timasheff, 1985). This technique is based upon the principle that the protein is completely excluded from the interior of the resin, while the ligand will be distributed throughout the solution. In the presence of a protein which binds the ligand, the establishment of chemical equilibrium will result in an apparent preferential exclusion of the ligand from the interior of the resin. Having determined the concentrations of PEP and PK before and after equilibrium is reached, we can combine these parameters to obtain the amount of bound and free PEP since

$$\alpha = (P/V_o)/(P/V) \tag{8.11}$$

where α is the ratio of protein concentrations, P is the total amount of protein added to the solution, V is the total volume of solution added to the dry gel, and V_o is the volume of solution outside the resin. P/V is the concentration of the protein added, assuming that it is equally distributed throughout the solution, while P/V_o is the observed concentration of the protein. Similarly

$$\beta = (L_o/V_o)/(L/V) \tag{8.12}$$

where β is the ratio of ligand concentrations and L and L_o are the total amount of ligand added and the amount of ligand outside the gel, respectively. L/V is the concentration of ligand, assuming it is evenly distributed in the total volume added, while L_o/V_o is the concentration of ligand observed in the gel-free solution. While β is the value of the ratio in the presence of protein, β' is the value in the absence of protein. The amount of bound ligand is

$$L_0(\text{bound}) = L(\beta - \beta')/(\alpha - \beta') \tag{8.13}$$

The concentration of free ligand outside the gel is

$$L_0(\text{free}) = (L/V)\beta'(\alpha - \beta)/(\alpha - \beta') \tag{8.14}$$

The amount of ligand bound per mole of RMPK tetramer is

$$Y = L_0(\text{bound})/P = (L/P)(\beta - \beta')/(\alpha - \beta') \tag{8.15}$$

For the specific practical aspects of preparing the resin and other details, the readers are referred to Oberfelder *et al.* (1984a). The ligand solutions are made up by dilution of a concentrated stock solution of ligand that had been spiked with either an aliquot of radioactively labeled ligand unless otherwise the ligand concentration can be detected accurately by other techniques. By making the solutions by serial dilution, it is assured that the final stock solutions had the same ratio of labeled to unlabeled ligand. After the gel is swollen, RMPK and radioactive ligand are added to the appropriate tubes. The tubes are again sealed tightly with parafilm and allowed to incubate in a temperature-controlled water bath at the desired temperature for 15 min. Samples are removed from the tubes with a 100-pL Hamilton syringe; this allowed the solution outside of the gel matrix to be sampled without contamination of gel beads.

7.2. Isothermal titration calorimetry

Isothermal titration calorimetry (ITC) experiments allow direct access to fundamental thermodynamic parameters associated with ligand binding and RMPK conformational transitions (Herman and Lee, 2009a). Since ITC experiments are not based on an enzymatic activity, binding of single ligands can be assessed and interaction between ligands investigated. A detailed description of the regulatory behavior of wild-type (WT) RMPK is essential for modeling its regulation under physiological conditions. It also creates an essential baseline for understanding perturbations induced by targeted genetic modifications of the recombinant enzyme.

Concentrations of RMPK ranged from 15 to 70 μ*M*. Stock solutions of 40 m*M* PEP, 100 m*M* Phe, and 100 m*M* ADP were used for injections. The titrants were prepared by dilution of the ligands in the dialyzate to prevent thermal effects caused by a buffer mismatch. The pH of the titrants was checked and adjusted, if necessary. When RMPK was titrated with Phe in the presence of a fixed concentration of ADP, the same concentration of ADP was present in the injectant. Typically, 15–25 aliquots of ligand were injected into a 1.4-mL sample. To correct data for heats of dilution of an injectant, a control experiment was performed under the same conditions except a buffer was substituted for the sample. The overall reaction heats were calculated by integration of the corrected ITC curves. The extent of irreversible processes caused by mixing of the protein at high temperatures in the calorimeter was also evaluated. Only an insignificant decrease of 3 ± 3% activity was observed after a 1-h calorimetric experiment at 40 °C.

To establish the energetic landscape of the regulatory behavior of RMPK in the presence of its ligands, we performed a series of ITC experiments at temperatures between 4 and 45 °C. To separate the contribution of the buffer ionization heat ΔH_{ion} from the overall reaction heat, we performed all titrations in two buffers with different ΔH_{ion} values.

7.3. Fluorescence

In order to rigorously test the validity of conclusions derived from the ITC data, a fluorescence approach, albeit indirect, that tracks continuous *structural* perturbations was employed (Herman and Lee, 2009b). Intrinsic Trp fluorescence of RMPK in the absence and in the presence of substrates PEP and ADP, and the allosteric inhibitor Phe was measured in the temperature range between 4 and 45 °C. For data analysis the fluorescence data were complemented by ITC experiments to obtain extended data set allowing more complete characterization of the RMPK regulatory mechanism. Twenty-one thermodynamic parameters were derived to define the network of linked interactions involved in regulating the allosteric behavior of RMPK through global analysis of the ITC and fluorescent data sets. *In this study, 27 independent curves with more than 1600 experimental points were globally analyzed.* Consequently, the consensus results not only substantiate the conclusions derived from the ITC data but also structural information characterizing the transition between the active and the inactive state of RMPK and the antagonism between ADP and Phe binding. The latter observation reveals a novel role for ADP in the allosteric regulation of RMPK.

7.4. Global fitting

Global analysis (Beechem *et al.*, 1983; Knutson *et al.*, 1983) is a powerful method for discerning between models and for accurate recovery of model parameters. The method is based on an ordinary nonlinear least-squares minimization (Marquardt, 1963) and allows for simultaneous analysis of multiple data sets. Data for the analysis can be acquired under different experimental conditions and with different techniques. Consequently, some model parameters are common for multiple curves. During global fitting, the overall sum of weighed squared deviations of measured values and values calculated from a model that encompasses all experimental data is minimized. Global analysis thus allows determination of parameter values that are consistent with all data sets. Importantly, linkage between particular parameters and different data sets sharpens the χ^2 surface with concomitant decrease of parameter correlation. Those parameters are recovered with higher accuracy (see Table 8.1; Herman and Lee, 2010). Over-determination of parameters, inherent to global analysis, helps to distinguish between alternative models by eliminating models inconsistent with data. The resolving power of global analysis is unequaled by a conventional nonlinear least-squares analysis. Global analysis has been previously used for large variety of experimental data and techniques (Ackers *et al.*, 1975; Beechem *et al.*, 1983; Eisenfeld and Ford, 1979; Johnson *et al.*, 1981; Oberfelder *et al.*, 1984a; Ucci and Cole, 2004; Verveer *et al.*, 2000). This approach of global analysis was applied to the data set obtained by ITC, fluorescence binding experiments, and fluorescence

Table 8.1 Parameters whose values are significantly improved by global fitting of the ITC and fluorescence data

Reaction	Parameter	Value		Unit[a]
		ITC	(ITC + fluorescence)	
Phe binding	$\Delta S_{\mathrm{Phe}}{}^{\mathrm{R}}$	7 (5)[b]	2.7 (0.9)	cal mol^{-1} K^{-1}
	$\Delta H_{\mathrm{Phe}}{}^{\mathrm{R}}$	0.9 (2.0)	−1.4 (0.4)	kcal mol^{-1}
	$\Delta S^{\mathrm{T}}{}_{\mathrm{Phe}}$	13 (7)	18.2 (0.2)	cal mol^{-1} K^{-1}
PEP binding	$\Delta S_{0,\,\mathrm{PEP}}{}^{\mathrm{R}}$	?	11.2 (0.2)	cal mol^{-1} K^{-1}
ADP–Phe coupling	$\Delta\Delta S^{\mathrm{T}}{}_{\mathrm{ADP,\,Phe}}$	−2.5 (2.0)	−4.9 (0.5)	cal mol^{-1} K^{-1}
	$R\Delta n_{\mathrm{ADP,\,Phe}}{}^{\mathrm{R}}$	−1.7 (1.0)[c]	−0.9 (0.5)	mol^{-1}[d]

[a] Per mol of a ligand.
[b] Standard deviations are given in parenthesis.
[c] Number of protons absorbed.
[d] Per mol of tetramer.

temperature scans for evaluation of the functional energetic landscape in the allosteric regulation of RMPK (Herman and Lee, 2009a,b). In all cases, the global analysis approach provided performance far beyond resolution of the conventional analysis. A more detail discussion on global fitting has recently been presented (Herman and Lee, 2010).

7.5. Results of global analysis of ITC and fluorescence data

7.5.1. Phe binding

The sign of heat exchange for the reaction changes from positive to negative during the titration. This is a clear indication that the reaction is complex and consists of at least two heat-generating processes with opposite signs. Actually, many reactions may contribute to the shape of ITC curves. The observation is consistent with the general mechanism of our model which includes binding to both enzyme states, a ligand induced shift of the R → T equilibrium accompanied by the change in the RMPK conformation, and linked proton reactions as described in our model. Heats resulting from reequilibration of ligands between the R and T states upon perturbation of the R → T equilibrium contribute to the detailed shape of the titration curves as well.

7.5.2. PEP binding

Since the patterns of the ITC data are quite complex, the consequence of linked multiple equilibria, a detailed interpretation of such curves is rather difficult. Therefore, we decided not to draw conclusions only on the basis of the shape of the ITC curves. Instead, at different temperatures, we titrated

RMPK to saturation, and the data are expressed as overall reaction heats. The results of this in-depth dissection of the thermodynamic signatures of RMPK interacting with metabolites provide novel insights into the mechanism of allosteric regulation of RMPK.

7.5.3. ADP binding

Binding of ADP to both states of RMPK was found to be strongly enthalpy driven with binding enthalpies to the R- and T-state about -10 and -13 kcal/mol, respectively. This is consistent with a binding mechanism that involves electrostatic interaction with the highly charged ADP substrate. Both entropy and enthalpy changes for binding of ADP were found to be the largest among all investigated ligands. ADP binding and the differential affinity toward the R- and T-states exhibit pronounced temperature dependence. The affinity to the T-state is larger at elevated temperatures. As a consequence, at high temperature ADP binds more favorably to the T-state resulting in shifting the R $\leftrightarrow$ T equilibrium toward the inactive T-state; thus, in this particular regard, ADP behaves like an inhibitor at high temperature. However, by virtue of its chemical structure, ADP is still a substrate of RMPK. In earlier studies, it was concluded that ADP behaves strictly as a substrate which plays a minor role in the allosteric regulation of RMPK because it does not show a differential affinity toward the two states of RMPK. However, as a consequence of extending the temperature range in this study, it is revealed that ADP actually plays a major role in the allosteric mechanism in RMPK under physiological relevant temperatures.

7.5.4. Energetic coupling between ADP–Phe bindings

Phe binding in the presence of ADP revealed that an antagonism exists between the two ligands, that is, Phe was found to bind more weakly in the presence of ADP. Due to the interaction enthalpy, $\Delta\Delta H^{T}_{\mathrm{ADP,\ Phe}}$ of about -0.5 kcal/mol, the enthalpy term $\Delta H^{T}_{\mathrm{ADP,\ Phe}} = \Delta H^{T}_{\mathrm{Phe}} + \Delta\Delta H^{T}_{\mathrm{ADP,\ Phe}}$ is reduced almost to zero. Concomitantly, the entropy change, $\Delta S^{T}_{\mathrm{ADP,\ Phe}} = \Delta S^{T}_{\mathrm{Phe}} + \Delta\Delta S^{T}_{\mathrm{ADP,\ Phe}}$ becomes smaller by 2.5 cal $\mathrm{mol}^{-1}\,\mathrm{K}^{-1}$. The net consequence of the coupling between ADP and Phe bindings is a reduction of the enthalpy term for Phe binding to essentially zero and a less favorable entropy term, that is, the presence of a bound ADP exerts a negative effect on Phe binding to the T-state. Thus, at high but physiologically relevant temperatures, the bound ADP modulates the inhibitory efficiency of Phe by reducing its affinity to the T-state.

7.5.5. Proton release or absorption

Information related to linked proton reactions associated with the ligand binding and the state transition is also available from Herman and Lee (2009a,b). The following reactions summarize these results:

Reactions with proton absorption:

$$0.2H^+ + PEP + R \rightleftarrows PEP \cdot R$$
$$0.5H^+ + R \rightleftarrows T$$
$$0.7H^+ + ADP + R \rightleftarrows ADP \cdot R$$
$$1.0H^+ + ADP + T \rightleftarrows ADP \cdot T$$

Reactions with proton release:

$$Phe + T \rightleftarrows Phe \cdot T + 0.9H^+$$
$$ADP + Phe + T \rightleftarrows ADP \cdot Phe \cdot T + 1.7H^+$$

Binding of substrates apparently always absorb protons, although the binding of ADP involves a larger amount of protons absorbed. Consequently, the binding of ADP would be more sensitive to pH perturbations. The R → T transition would also absorb protons. For the reactions which involve in proton absorption, lower pH would shift the equilibria to the right, as defined by the Le Chatelier's principle. Thus, lower pH would favor the bindings of ADP, PEP, and the T-state. The net result would be an expected change in cooperativity in substrate binding, the extent of which is pH dependent.

In contrast, binding of Phe to the T-state, in the presence or absence of ADP, leads to release of protons. Another significant observation is that the amount of proton released almost doubles in the presence of ADP. If the bindings of Phe and ADP were simply a summation of the two reactions (absorption of 0.7 and release of 0.9 H^+ for ADP and Phe binding, respectively), then the net amount of proton release is expected to be about zero; however, instead the observation is a doubling of H^+ release to 1.7. This is a clear indication of the coupling of the two binding events. Binding of Phe and ADP to the T-state seems to be more pH dependent.

These results clearly indicate that the effect of pH on the basic allosteric behavior of RMPK is a composite of the nature and magnitude of proton release or absorption linked to the various reactions. According to the Wyman's linked-function theory (1964) there should be dependence of dissociation constants on a concentration of protons and shift of the R ↔ T equilibrium. For example, at low pH the T-state is favored but the binding of Phe would be weakened. Thus, a binding isotherm of Phe is pH dependent as a function of the relative values of equilibrium constants which define the distribution of the R- and T-state and the relative affinities of Phe to these states. Simultaneously, the affinity of substrates would be affected. Thus, one should expect that the allosteric behavior of RMPK is a complex phenomenon defined by the specific experimental conditions. It is most gratifying to note that such an expectation was reported by Consler

et al. (1990). Based on steady-state kinetic studies, these authors reported the synergistic effects of proton and Phe on the regulation of RMPK.

7.5.6. Comment on the results derived from global fitting of both fluorescence and ITC data sets

Table 8.1 summarizes the results of the improvements of parameters when both sets of data were analyzed. It is clear that not only the specific values of the parameters are more accurate; the standard errors have improved significantly. These are solid proofs of the value and power of global analysis on multiple sets of data, particularly data sets collected from different techniques.

A summary of this binding study:

- The state of RMPK that ADP preferentially binds is temperature-dependent. ADP binds more favorably to the T and R states at high and low temperatures, respectively. This crossover of affinity toward the R and T states implies that ADP not only serves as a substrate but also plays an important and intricate role in regulating RMPK activity.
- The binding of Phe is negatively coupled to that of ADP in addition to the shifting of the R $\rightarrow$ T equilibrium due to the relative affinities of Phe or ADP for these two states; that is, the assumption that ligand binding to RMPK is state-dependent is only correct for PEP but not Phe in the presence of ADP.
- The release or absorption of protons linked to the various equilibria is specific to the particular reaction. As a consequence, pH will exert a complex effect on these linked equilibria, with the net effect being manifested in the regulatory behavior of RMPK.
- The R $\rightarrow$ T equilibrium is accompanied by a significant ΔCp.

Our conclusions derived from calorimetric data are in full agreement with those based on our published steady-state kinetic studies. These conclusions are further strengthened by our fluorescence data and model simulations (Herman and Lee, 2009b,c).

8. Protein Structural Dynamics—Amide Hydrogen Exchange Monitored by FT-IR (HX-FT-IR)

We further studied the structural perturbations by Fourier transform infrared (FT-IR) spectroscopy (Yu *et al.*, 2003). The experiments were designed to monitor the secondary structure of RMPK in the presence of saturating amounts of various ligands. Mg^{2+} is a divalent cation essential for activity. PEP and ADP are the two substrates while Phe is the inhibitor. In all

experimental conditions, there is no significant change in the areas encompassed by the peaks assigned to either α or β structures. That implies that there is no detectable conversion of secondary structure of RMPK in the presence of all these ligands. A closer examination of the data shows that the maximum wavenumber associated with α-helix remains the same while that of the β-strand shifts as a function of ligand. In the presence of Mg^{2+}, PEP and ADP the maximum wavenumber is less than that in buffer alone or Phe. These results imply that the local environments of the β-strands are perturbed by these ligands, although the amount of β strands has not changed. The origin of the differential perturbations by ligands in the environments of secondary structures might be the modulation of structural dynamics of RMPK. Thus, the structural dynamics of RMPK in the presence of various ligands was probed by H/D exchange monitored by FT-IR. The second derivative spectra as a function of time of H/D exchange were monitored and compared. The spectra in the presence of K^+ and Mg^{2+} were compared to those of RMPK in buffer. They show that the basic pattern of exchange was retained. However, a larger change in intensity was observed even at the 1-min time point. These results imply that the activating metal ions induce an increase in the number of rapidly exchangeable amide protons. The presence of either PEP or ADP shows a pattern of exchange that is quite similar to each other, namely, a very rapid exchange was observed in both the helices and sheets. There is a clear indication of the presence of two different populations of helices. The change in the second derivative spectra reflecting the amide proton exchange in the presence of Phe showed that within the time frame of the experiment no exchangeable amide proton was detected in the β-sheets, an observation that differs from that of the helices. Thus, these H/D exchange experiments show that substrates (ADP or PEP) and activating metal ions (Mg^{2+}) lock RMPK in a more dynamic E^R structure while Phe exerts an opposite effect.

These results provide the first evidence for a differential effect of ligand binding on the dynamics of the structural elements, not major conformational changes, in RMPK. These data are consistent with our model that allosteric regulation of RMPK is the consequence of perturbation of the equilibrium of an ensemble of states the distribution of which resides mainly around the two extreme dominant end states. Sequence differences and ligands can modulate the distribution of states leading to alterations of functions.

9. Probing Interfacial Interactions

9.1. S402P mutation in the interface between the C-domains

In RMPK, there are two intersubunit interfaces—one between the C-domains while the other is between the A-domains. In order to probe the interfacial interactions, we mutated residue 402 of RMPK from S to P, in

accordance to the difference in sequence between the muscle and kidney isozymes. Converting S402 to P changes neither the secondary, nor the tetrameric structure (Friesen *et al.*, 1998a). The S402P RMPK mutant exhibits steady-state kinetic behavior that indicates that it is more responsive to regulation by effectors. The sigmoidicity of the curves (activity vs. substrate concentration) is a reflection of cooperativity of substrate binding. The RMPK data show almost no sigmoidicity, as expected for an enzyme exhibiting little allosteric behavior; whereas the rabbit kidney PK shows pronounced sigmoidicity. The data for the S402P RMPK are intermediary to the muscle and kidney isozymes. The presence of 12 m*M* inhibitor Phe shifts the curve to the right, as expected, since Phe would shift the conformational state equilibrium toward E^T which has a weaker affinity for PEP. The presence of 10 n*M* activator FBP in addition to 12 m*M* Phe shifts the curve to the left. In RMPK, without the inhibitory effect of 12 m*M* Phe, it would still require millimolar concentrations of FBP to achieve the same effect. Thus, an S402P mutation confers partial restoration of allosteric behavior to the RMPK.

We have elucidated the atomic structure of the S402P RMPK variant by X-ray crystallography (Wooll *et al.*, 2001). Although the overall S402P RMPK structure is nearly identical to the WT structure within experimental error, significant differences in the conformation of the backbone are found at the site of mutation. We found that the ratio of B-factors of mutant/WT provides a good representation of the pattern of long range communications between distant sites (Wooll *et al.*, 2001). The most obvious *increase in B-factor* in the S402P RMPK is around the residue 402 indicating a significant increase in dynamics in that region. There are also significant changes in the ratio of B-factor for residues 50–200. In addition, there is an increase in the number of heterogeneity in the angle assumed by the B-domain with respect to the A-domain, that is, *increases dynamics in domain movements*. Closer examination of the X-ray data shows a disruption of a salt bridge between residues 341 and 177 of an adjacent subunit. This salt bridge and residue 402 reside in different subunit interfaces. Thus, these structural data show a communication between these two different subunit interfaces. A similar conclusion was derived from the results of our study of subunit assembly (Friesen and Lee, 1998; Friesen *et al.*, 1998b). It is evident that a mutation at residue 402 leads to *increased dynamics in distant sites through long range communication without significant changes in secondary structures*.

9.2. T340M mutation along the interface between the A-domains

In an effort to establish functional coupling among residues in RMPK, we incorporated into our studies the human genetic data (Baronciani and Beutler, 1995; Kanno *et al.*, 1991; Miwa *et al.*, 1993; Neubauer *et al.*,

1991; Valentine *et al.*, 1989). Our choice of residue 340 is based on the combined results of our structural studies and human genetic data. In our modeling study, we have further identified the residues whose inter-α carbon distances are within 15 Å (Consler *et al.*, 1994) along the axis between the adjacent A-domains. These include residues 330–350. Human genetic data identified T340M as a mutant which is observed in patients suffering from PK deficiency. The T340M RMPK and RKPK (kidney isozyme of PK) mutants are only half as active as the WT PKs. The T340M RMPK enzyme is more susceptible than RKPK to inhibition by Phe or to the activator FBP. The differences in the amino acid sequence of RMPK and RKPK are only 22 amino acids, all of which reside in the C-domain. Evidently the 22 residues in the C-domain modulate the effect of residue 340, which reside in different subunit interfaces. The resultant is a differential effect on the functional energetics of PK. This study demonstrates the linkage between distant residues in different interfacial interactions, that is, establishing the functional coupling among residues and the identities of these residues.

10. Summary Statement

The understanding of the molecular mechanisms of allostery in PK is still in its infancy. A vast amount of knowledge has been acquired; however, we have yet to identify the chemical principles underlying the observations. We do not understand the molecular mechanism that leads to the change in allosteric behavior due to mutations, the communication pathway and the thermodynamic parameters that drive the allosteric behavior. A current view of protein indicates that it is an ensemble of microstates in equilibrium (Ferreon *et al.*, 2003; Friere, 1999; Hilser *et al.*, 1998, 2006; Liu *et al.*, 2006; Luque *et al.*, 2002; Pan *et al.*, 2000; Schrank *et al.*, 2009). Mutations, change in solvent environment or binding of ligands lead to a redistribution of these microstates. The biological activity is a manifestation of the functional properties of the dominant state(s). The present knowledge of the allosteric properties of RMPK seems to favor that hypothesis, in particular, in view of the plasticity of the orientations of the B domain with respect to the A domain (Wooll *et al.*, 2001) and the small angle X-ray scattering (SAXS) results of different structures of RMPK in complex with different amino acids as inhibitors (Fenton *et al.*, 2010). The tetrameric PK is a particularly attractive model system to elucidate the ground rules of allostery. There are four isozymes and each has its own specific allosteric behavior. The sequences of some of these isozymes consist of a small number of changes, for example, only 22 amino acids out of 530 in each subunit are different between the muscle and kidney isozymes. Furthermore, these different

amino acids are clustered in one domain. Thus, embedded in these two isoforms of PK are the rules involved in engineering the popular TIM $(\alpha/\beta)_8$ motif to modulate its allosteric properties.

ACKNOWLEDGMENTS

Supported by NIH GM 77551 and the Robert A. Welch Foundation (J. C. L.) and grant MSM 0021620835 of the Ministry of Education Youth and Sports of the Czech Republic (P. H.).

REFERENCES

Ackers, G. K. (1970). Analytical gel chromatography of proteins. *Adv. Protein Chem.* **24,** 343–446.

Ackers, G. K., Johnson, M. L., Mills, F. C., Halvorson, H. R., and Shapiro, S. (1975). The linkage between oxygenation and subunit dissociation in human hemoglobin. Consequences for the analysis of oxygenation curves. *Biochemistry* **14,** 5128–5134.

Ainsworth, S., and MacFarlane, N. (1973). A kinetic study of rabbit muscle pyruvate kinase. *Biochem. J.* **131,** 223–236.

Baronciani, L., and Beutler, E. (1995). Molecular study of pyruvate kinase deficient patients with hereditary nonspherocytic hemolytic anemia. *J. Clin. Invest.* **95,** 1702–1709.

Beechem, J. M., Knutson, J. R., Ross, J. B. A., Turner, B. W., and Brand, L. (1983). Global resolution of heterogeneous decay by phase modulation fluorometry—Mixtures and proteins. *Biochemistry* **22,** 6054–6058.

Consler, T. G., Uberbacher, E. C., Bunick, G. J., Liebman, M. N., and Lee, J. C. (1988). Domain interaction in rabbit muscle pyruvate kinase. II. Small angle neutron scattering and computer simulation. *J. Biol. Chem.* **263,** 2794–2801.

Consler, T. G., Woodard, S. H., and Lee, J. C. (1989). Effects of primary sequence differences on the global structure and function of an enzyme: A study of pyruvate kinase isozymes. *Biochemistry* **28,** 8756–8764.

Consler, T. G., Jennewein, M. J., Cai, G.-Z., and Lee, J. C. (1990). Synergistic effects of proton and phenylalanine on the regulation of muscle pyruvate kinase. *Biochemistry* **29,** 10765–10771.

Consler, T. G., Jennewein, M. J., Cai, G. Z., and Lee, J. C. (1992). Energetics of allosteric regulation in muscle pyruvate kinase. *Biochemistry* **31,** 7870–7878.

Consler, T. G., Liebman, M. N., and Lee, J. C. (1994). Structural elements involved in the allosteric switch in mammalian pyruvate kinase. *In* "Molecular Modeling," (M. N. Liebman and T. Kumosinski, eds.), pp. 466–485, Chapter 25.

Copley, R. R., and Bork, P. (2000). Homology among $(\beta\alpha)_8$ barrels: Implications for the evolution of metabolic pathways. *J. Mol. Biol.* **303,** 627–640.

Debye, P. (1915). Zerstreuung von Rontgenstrahlen. *Ann. Phys. (Leipzig)* **46,** 809–823.

Dombrauckas, J. D., Santarsiero, B. D., and Mesecar, A. D. (2005). Structural basis for tumor pyruvate kinase M2 allosteric regulation and catalysis. *Biochemistry* **44,** 9417–9429.

Eisenfeld, J., and Ford, C. C. (1979). A systems-theory approach to the analysis of multiexponential fluorescence decay. *Biophys. J.* **26,** 73–83.

Farber, G. K., and Petsko, G. A. (1990). The evolution of α/β barrel enzymes. *Trends Biochem. Sci.* **15,** 228–234.

Fenton, A. W., and Alontaga, A. Y. (2009). The impact of ions on allosteric functions in human liver pyruvate kinase. *Methods Enzymol.* **466,** 83–107.
Fenton, A. W., and Hutchison, M. (2009). The pH dependence of the allosteric response of human liver pyruvate kinase to fructose-1,6-bisphosphate, ATP and alanine. *Arch. Biochem. Biophys.* **484,** 16–23.
Fenton, A. W., Williams, R., and Trewhella, J. (2010). Changes in small-angle X-ray scattering parameters observed upon binding of ligand to rabbit muscle pyruvate kinase are not correlated with allosteric transitions. *Biochemistry* **49,** 7202–7209.
Ferreon, J. C., Volk, D. E., Luxon, B. A., Gorenstein, D. G., and Hilser, V. J. (2003). Solution structure, dynamics, and thermodynamics of the native state ensemble of the Sem-5 C-terminal SH3 domain. *Biochemistry* **42,** 5582–5591.
Friere, E. (1999). The propagation of binding interactions to remote sites in proteins: Analysis of the binding of the monoclonal antibody D1.3 to lysozyme. *Proc. Natl. Acad. Sci. USA* **96,** 10118–10122.
Friesen, R. H. E., and Lee, J. C. (1998). The negative dominant effects of T340M mutation on mammalian pyruvate kinase. *J. Biol. Chem.* **273,** 14772–14779.
Friesen, R. H. E., Castellani, R. J., Lee, J. C., and Braun, W. (1998a). Allostery in rabbit pyruvate kinase: Development of a strategy to elucidate the mechanism. *Biochemistry* **37,** 15266–15276.
Friesen, R. H. E., Chin, A. J., Ledman, D. W., and Lee, J. C. (1998b). Interfacial communications in recombinant rabbit kidney pyruvate kinase. *Biochemistry* **37,** 2949–2960.
Gerhart, J. C., and Schachman, H. K. (1968). Allosteric interactions in aspartate transcarbamylase. II. Evidence for different conformational states of the protein in the presence and absence of specific ligands. *Biochemistry* **7,** 538–552.
Gerlt, J. A., and Babbitt, P. C. (2001). Divergent evolution of enzymatic function: Mechanistically diverse superfamilies and functionally distinct superfamilies. *Annu. Rev. Biochem.* **70,** 209–246.
Hall, E. R., and Cottam, G. L. (1978). Isozymes of pyruvate kinase in vertebrates: Their physical, chemical, kinetic and immunological properties. *Int. J. Biochem.* **9,** 785–793.
Harris, S. J., and Winzor, D. J. (1998). Thermodynamic nonideality as a probe of allosteric mechanisms: Preexistence of the isomerization equilibrium for rabbit muscle pyruvate kinase. *Arch. Biochem. Biophys.* **265,** 458–465.
Heggi, H., and Gerstein, M. (1999). The relationship between protein structure and function: A comprehensive survey with application to the yeast genome. *J. Mol. Biol.* **288,** 147–164.
Herman, P., and Lee, J. C. (2009a). Functional energetic landscape in the allosteric regulation of muscle pyruvate kinase I. Calorimetric study. *Biochemistry* **48,** 9448–9455.
Herman, P., and Lee, J. C. (2009b). Functional energetic landscape in the allosteric regulation of muscle pyruvate kinase II. Fluorescence study. *Biochemistry* **48,** 9456–9465.
Herman, P., and Lee, J. C. (2009c). Functional energetic landscape in the allosteric regulation of muscle pyruvate kinase. III. Mechanism. *Biochemistry* **48,** 9466–9470.
Herman, P., and Lee, J. C. (2010). The advantage of global fitting of data involving complex linked reactions. *Methods Mol. Biol.* (in press).
Heyduk, E., Heyduk, T., and Lee, J. C. (1992). Global conformational changes in allosteric proteins. *J. Biol. Chem.* **267,** 3200–3204.
Hilser, V. J., Dowdy, D., Oas, T. G., and Freire, E. (1998). The structural distribution of cooperative interactions in proteins: Analysis of the native state ensemble. *Proc. Natl. Acad. Sci. USA* **95,** 9903–9908.
Hilser, V. J., Garcia-Moreno, E. B., Oas, T. G., Kapp, G., and Whitten, S. T. (2006). A statistical thermodynamic model of the protein ensemble. *Chem. Rev.* **106,** 1545–1558.
Hirose, M., and Kano, Y. (1971). Binding of ligands by proteins: A simple method with sephadex gel. *Biochim. Biophys. Acta* **251,** 376–379.

Holt, J. M., and Ackers, G. K. (1995). Pathway of allosteric control as revealed by intermediate states of hemoglobin. *Methods Enzymol.* **259,** 1–19.

Howlett, G. J., and Schachman, H. K. (1977). Allosteric regulation of aspartate transcarbamoylase. Changes in the sedimentation coefficient promoted by the bisubstrate analogue *N*-(phosphonacetyl)-L-aspartate. *Biochemistry* **16,** 5077–5083.

Johnson, M. L., Correia, J. J., Yphantis, D. A., and Halvorson, H. R. (1981). Analysis of data from the analytical ultracentrifuge by nonlinear least-squares techniques. *Biophys. J.* **36,** 575–588.

Kanno, H., Fujii, H., Hirono, A., and Miwa, S. (1991). cDNA cloning of human r-type pyruvate kinase and identification of a single amino acid substitution ($Thr^{384} \rightarrow Met$) affecting enzymatic stability in a pyruvate kinase variant (PK Tokyo) associated with hereditary hemolytic anemia. *Proc. Natl. Acad. Sci. USA* **88,** 8218–8221.

Kayne, F. (1973). Pyruvate kinase. *In* "The Enzymes," (P. D. Boyer, ed.), 3rd ed. p. 353. Academic Press, New York.

Kayne, F. J., and Price, N. C. (1972). Conformational changes in the allosteric inhibition of muscle pyruvate kinase by phenylalanine. *Biochemistry* **11,** 4415–4420.

Knutson, J. R., Beechem, J. M., and Brand, L. (1983). Simultaneous analysis of multiple fluorescence decay curves—A global approach. *Chem. Phys. Lett.* **102,** 501–507.

Koshland, D. E., Jr., Nemethy, G., and Filmer, D. (1966). Comparison of experimental binding data and theoretical models in proteins containing subunits. *Biochemistry* **5,** 365–385.

Kwan, C. Y., and Davis, R. C. (1980). pH-dependent amino acid induced conformational changes of rabbit muscle pyruvate kinase. *Can. J. Biochem.* **58,** 188–193.

Kwan, C. Y., and Davis, R. C. (1981). L-Phenylalanine induced changes of sulfhydryl reactivity in rabbit muscle pyruvate kinase. *Can. J. Biochem.* **59,** 92–99.

Larsen, T. M., Laughlin, T., Holden, H. M., Rayment, I., and Reed, G. H. (1994). Structure of rabbit muscle pyruvate kinase complexed with Mn^{2+}, K^+, and pyruvate. *Biochemistry* **33,** 6301–6309.

Larsen, T. M., Benning, M. M., Wesenberg, G. E., Rayment, I., and Reed, G. H. (1997). Ligand-induced domain movement in pyruvate kinase: Structure of the enzyme from rabbit muscle with Mg^{2+}, K^+, and l-phospholactate at 2.7 Å resolution. *Arch. Biochem. Biophys.* **345,** 199–206.

Larsen, T. M., Benning, M. M., Rayment, I., and Reed, G. H. (1998). Structure of the bis (Mg^{2+})-ATP-oxalate complex of the rabbit muscle pyruvate kinase at 2.1 Å resolution: ATP binding over a barrel. *Biochemistry* **37,** 6247–6255.

Liu, T., Whitten, S. T., and Hilser, V. J. (2006). Ensemble-based signatures of energy propagation in proteins: A new view of an old phenomenon. *Proteins Struct. Funct. Bioinform.* **62,** 728–738.

Luque, I., Leavitt, S. A., and Freire, E. (2002). The linkage between protein folding and functional cooperativity: Two sides of the same coin? *Annu. Rev. Biophys. Biomol. Struct.* **31,** 235–256.

Marquardt, D. W. (1963). An algorithm for least-squares estimation of nonlinear parameters. *J. Soc. Ind. Appl. Math.* **11,** 431–441.

Mattevi, A., Valentini, G., Rizzi, M., Speranza, M. L., Bolognesi, M., and Coda, A. (1995). Crystal structure of *E. coli* pyruvate kinase type I: Molecular basis of the allosteric transition. *Structure* **3,** 729–741.

Mattevi, A., Bolognesi, M., and Valentini, G. (1996). The allosteric regulation of pyruvate kinase. *FEBS Lett.* **289,** 15–19.

Mesecar, A. D., and Nowak, T. (1997a). Metal-ion-mediated allosteric triggering of yeast pyruvate kinase. 1. A multidimensional kinetic linked-function analysis. *Biochemistry* **36,** 6792–6802.

Mesecar, A. D., and Nowak, T. (1997b). Metal-ion-mediated allosteric triggering of yeast pyruvate kinase. 2. A multidimensional thermodynamic linked-function analysis. *Biochemistry* **36,** 6803–6813.

Miwa, S., Kanno, H., and Fujii, H. (1993). Concise review: Pyruvate kinase deficiency: Historical perspective and recent progress of molecular genetics. *Am. J. Hematol.* **42,** 31–35.

Monod, J., Wyman, J., and Changeux, J. P. (1965). On the nature of allosteric transitions: A plausible model. *J. Mol. Biol.* **12,** 88–118.

Moore, P. B. (1980). Small-angle scattering. Information content error analysis. *J. Appl. Cryst.* **13,** 168–175.

Na, G. C., and Timasheff, S. N. (1985). Measurement and analysis of ligand-binding isotherms linked to protein self-association. *Methods Enzymol.* **117,** 496–519.

Neubauer, B., Lakomek, M., Winkler, H., Paske, M., Hofferbert, S., and Schröter, W. (1991). Point mutations in the L-type pyruvate kinase gene of two children with homolytic anemia caused by pyruvate kinase deficiency. *Blood* **77,** 1871–1875.

Oberfelder, R. W., Lee, L. L., and Lee, J. C. (1984a). Thermodynamic linkages in rabbit muscle pyruvate kinase: Kinetic, equilibrium, and structural studies. *Biochemistry* **23,** 3813–3821.

Oberfelder, R. W., Barisas, B. G., and Lee, J. C. (1984b). Thermodynamic linkages in rabbit muscle pyruvate kinase: Analysis of experimental data by a two-state model. *Biochemistry* **23,** 3822–3826.

Pan, H., Lee, J. C., and Hilser, V. J. (2000). Binding sites in *Escherichia coli* dihydrofolate reductase communicate by modulating the conformational ensemble. *Proc. Natl. Acad. Sci. USA* **97,** 12020–12025.

Reinhart, G. D. (2004). Quantitative analysis and interpretation of allosteric behavior. *Methods Enzymol.* **380,** 187–203.

Schrank, T. P., Bolen, D. W., and Hilser, V. J. (2009). Rational modulation of conformational fluctuations in adenylate kinase reveals a local unfolding mechanism for allostery and functional adaptation in proteins. *Proc. Natl. Acad. Sci. USA* **106,** 16984–16989.

Siegel, L., and Monty, K. J. (1966). Determination of molecular weights and frictional ratios of proteins in impure systems by use of gel filtration and density gradient centrifugation. Application to crude preparations of sulfite and hydroxylamine reductases. *Biochim. Biophys. Acta* **112,** 346–362.

Steinhardt, J., and Reynolds, J. A. (1969). Multiple Equilibria in Proteins. Academic Press, New York, NY.

Stuart, H., Levine, M., Muirhead, H., and Stammers, D. K. (1979). Crystal structure of cat muscle pyruvate kinase at a resolution of 2·6 Å. *J. Mol. Biol.* **134,** 109–142.

Suelter, C. H., Singleton, R., Jr., Kayne, F. J., Arrington, S., Glass, J., and Mildvan, A. S. (1966). Studies on the interaction of substrate and monovalent and divalent cations with pyruvate kinase. *Biochemistry* **5,** 131–139.

Tanford, C. (1969). Extension of the theory of linked function to incorporate the effects of protein hydration. *J. Mol. Biol.* **39,** 539–544.

Ucci, J. W., and Cole, J. L. (2004). Global analysis of non-specific protein–nucleic interactions by sedimentation equilibrium. *Biophys. Chem.* **108,** 127–140.

Valentine, W. N., Tanaka, K. R., and Paglia, D. E. (1989). Pyruvate kinase and other enzyme deficiency disorders of the erythrocyte. *In* "The Metabolic Basis of Inherited Disease, Vol. 6," (C. R. Seriver, A. L. Beaudet, W. S. Sly, and D. Valle, eds.). McGrans-Hill, New York.

Verveer, P. J., Squire, A., and Bastiaens, P. I. (2000). Global analysis of fluorescence lifetime imaging microscopy data. *Biophys. J.* **78,** 2127–2137.

Weber, G. (1972). Ligand binding and internal equilibria in proteins. *Biochemistry* **11,** 864–878.

Wierenga, R. K. (2001). The TIM-barrel fold: A versatile framework for efficient enzymes. *FEBS Lett.* **492,** 193–198.

Williams, R., Holyoak, T., McDonald, G., Gui, C., and Fenton, A. W. (2006). Differentiating a ligand's chemical requirements for allosteric interactions from those for protein binding. Phenylalanine inhibition of pyruvate kinase. *Biochemistry* **45,** 5421–5429.

Wooll, J. O., Friesen, R. H. E., White, M. A., Watowich, S. J., Fox, R. O., Lee, J. C., and Czerwinski, E. W. (2001). Structural and functional linkages between subunit interfaces in mammalian pyruvate kinase. *J. Mol. Biol.* **312,** 525–540.

Wyman, J. (1964). Linked functions and reciprocal effects in hemoglobin: A second look. *Adv. Prot. Chem.* **19,** 223–286.

Wyman, J., and Gill, S. J. (1990). Bing and Linkage: Functional Chemistry of Biological Macromolecules. University Science Books, Mill Valley, CA.

Yu, S., Lee, L., and Lee, J. C. (2003). Effects of metabolites on the structural dynamics of rabbit muscle pyruvate kinase. *Biophys. Chem.* **103,** 1–11.